



Australian Government
Bureau of Meteorology

The Centre for Australian Weather and Climate Research
A partnership between CSIRO and the Bureau of Meteorology

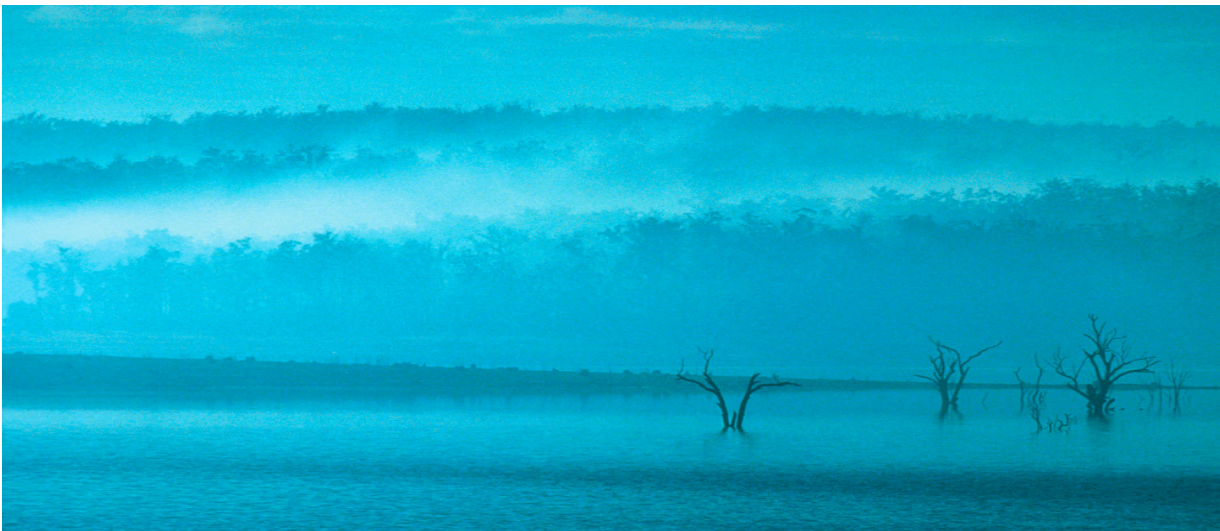


Improvements in POAMA2 for the prediction of major climate drivers and south eastern Australian rainfall

Eun-Pa Lim, Harry H. Hendon, Sally Langford and Oscar Alves

CAWCR Technical Report No. 051

May 2012



www.cawcr.gov.au



Improvements in POAMA2 for the prediction of major climate drivers and south eastern Australian rainfall

Eun-Pa Lim, Harry H. Hendon, Sally Langford and Oscar Alves

*The Centre for Australian Weather and Climate Research
- a partnership between CSIRO and the Bureau of Meteorology*

CAWCR Technical Report No. 051

May 2012

ISSN: 1836-019X

National Library of Australia Cataloguing-in-Publication entry

Author: Eun-Pa Lim, Harry H. Hendon, Sally Langford and Oscar Alves

Title: Improvements in POAMA2 for the prediction of major climate drivers and south eastern Australian rainfall

ISBN: 9780643108417 (Electronic Resource)

Series: CAWCR technical report; 51

Subjects: Meteorology--Australia, Southeastern.

Weather forecasting--Australia, Southeastern.

Australia, Southeastern--Climate.

Notes: Included bibliography references and index

Other Authors / Contributors: Day, K.A. (Editor)

Dewey Number: 551.63

Enquiries should be addressed to:

Dr. Eun-Pa Lim,
Centre for Australian Weather and Climate Research,
GPO Box 1289,
Melbourne, VIC, 3001
AUSTRALIA
email: E.Lim@bom.gov.au

Copyright and Disclaimer

© 2012 CSIRO and the Bureau of Meteorology. To the extent permitted by law, all rights are reserved and no part of this publication covered by copyright may be reproduced or copied in any form or by any means except with the written permission of CSIRO and the Bureau of Meteorology.

CSIRO and the Bureau of Meteorology advise that the information contained in this publication comprises general statements based on scientific research. The reader is advised and needs to be aware that such information may be incomplete or unable to be used in any specific situation. No reliance or actions must therefore be made on that information without seeking prior expert professional, scientific and technical advice. To the extent permitted by law, CSIRO and the Bureau of Meteorology (including each of its employees and consultants) excludes all liability to any person for any consequences, including but not limited to all losses, damages, costs, expenses and any other compensation, arising directly or indirectly from using this publication (in part or in whole) and any information or material contained in it.

Contents

Introduction	1
1. POAMA2	2
2. Results	4
2.1 Prediction of climate drivers.....	4
2.2 Impact of flux correction.....	9
2.3 SEA rainfall forecasts	15
2.4 Comparison with ENSEMBLES and a true MME	17
3. Concluding remarks	19
4. Acknowledgments	20
5. References	21

List of Figures

Fig. 1 (a)-(c) Regression patterns (right) of observed SST onto the observed times series of the NINO3, EMI and DMI indices (left) for the period of 1980-2010. (d) Regression pattern of observed MSLP (right) onto the observed SAM index (left) for the same period.....	4
Fig. 2 Climate drivers with highest correlation with rainfall at each grid point (left) and correlation of NINO3 (green), EMI (blue), DMI (red), and SAM index (yellow) with SEA area-averaged rainfall (right) over the period of 1980-2010.....	5
Fig. 3 Forecast skill of key climate drivers Nino3, EMI, IOD, and the SAM. Coloured lines are the forecast skill over 1980-2006, and black lines are the forecast skill over 1960-2010. Forecast skill is assessed by correlation between forecasts and observation of each index.....	6
Fig. 4 Forecast skill (correlation between forecasts and observation) difference between POAMA1.5 and POAMA2 (POAMA2 minus POAMA1.5) as a function of forecast start time and lead time. Pink (blue) colour shading indicates POAMA2 skill to be higher (lower) than that of POAMA1.5.....	7
Fig. 5 (a) POAMA2 and (b) persistence forecast skill (as measured by correlation) of SAM as a function of forecast start time and lead time. (c) Observed correlation between monthly SAM and NINO3 in 1980-2010.	8
Fig. 6 Forecast skill (as measured by correlation) for major climate drivers at lead time zero month (upper panel) and three months (lower panel). The verification season (3 month mean) is along the x-axis.....	9
Fig. 7 SST mean state bias at 0 and 6 month lead times in POAMA1.5, each version of POAMA2 and the finally configured POAMA2 consisting of the three versions of POAMA2. Blue colour indicates predicted climatological SST to be colder than the observed over the period of 1980-2006. Contour interval is 0.5 °C.	10
Fig. 8 (a) SST patterns of cold-tongue El Niño (left) and warm-pool El Niño (right), (b) pattern correlation between cold-tongue and warm-pool El Niños in the observation (dashed line), and non flux corrected (p24a; blue line) and flux corrected (p24b; red line) forecasts, (c) pattern correlation between predicted and observed cold-tongue El Niño, and (d) the same as (c) but for warm-pool El Niño, (e) overlapped plot of (b) and (d). In (e) the cross point of the solid and dashed lines indicates the lead time when the model predicted cold-tongue and warm-pool El Niños start to be more alike to each other than to their observed counterparts.....	11
Fig. 9 Correlation of June-July-August Australian rainfall with (a) the NINO3 index and (b) the EMI in the observation and in the non-flux corrected and flux corrected forecasts at lead time of 0-4 months over the period of 1980-2010. (c) Forecast skill (as measured by correlation) of winter rainfall at 0-2 month lead time.	13
Fig. 10 (a) Observed seasonal cycle of subtropical ridge (STR) mean position (y-axis) and intensity (x-axis) and their correlation with the southern part of SEA rainfall (south of 32°S) superimposed on the cycle at each season. Blue circle (red open circle with x) represents the correlation with STR intensity (position). In the legend the small and big blue circles represents 0.4 and 0.6 correlation, respectively, (b) Representation of STR mean intensity and position and prediction skill of the variabilities of STR intensity and position in non-flux corrected (upper row) and flux corrected (bottom row) forecasts at lead times of 0, 2, 4, and 6 months. Solid grey line represents observed seasonal cycle whereas dotted black line represents predicted seasonal cycle. Blue circle (red open circle) indicates skill to predict STR intensity (position) variability. Dot size is proportional	

to the magnitude of correlation coefficient. The size of the circles in the legend represent 0.4 correlation.	14
Fig. 11 Proportion of correct forecasts (expressed in percentage) of predicting seasonal rainfall to be above the median in POAMA1.5 (left column), POAMA2 (middle column) and calibrated POAMA2 (right column) at (a) LT 0 and (b) LT 3 months. Colour shading is 10% interval.	16
Fig. 12 Attributes diagrams of POAMA1.5, POAMA2 and calibrated POAMA2 forecasts of above median rainfall, considering the forecasts over all grid points of SEA for all 12 seasons in 1980-2006 at LT 0 (upper panels) and LT 3 months (lower panels). Perfectly reliable forecasts should line up with the diagonal line. Forecasts in the grey areas are considered to be reliable as they are correct in predicting the occurrence/non-occurrence of an event (in this study, above median rainfall) and their errors are smaller than a climatological forecast. The size of dots represents forecast frequency in each probabilistic forecast category.	17
Fig. 13 (a) Proportion of correct forecasts and (b) attributes diagrams of predicting seasonal rainfall over SEA to be above the median in ECMWF system3, POAMA2, calibrated POAMA2 and a multi-model ensemble system consisting of POAMA2, ECMWF, UK Met Office, and Meteo-France forecast systems at 1 month lead time.....	18

INTRODUCTION

Ocean-atmosphere interactions are key processes that drive seasonal climate variability. In the global sense, the atmosphere drives the upper ocean via heat flux, fresh water flux and wind stress (Anderson 2008). But in the tropics where the ocean surface temperature (hereafter, sea surface temperature, SST) is warm enough to trigger deep atmospheric convection, the ocean exerts strong controls on the atmosphere especially at longer time scales because of its slow variations and strong thermal inertia. Consequently, the highest predictability of atmospheric climate (e.g. temperature and rainfall) on seasonal timescales is found predominantly across and directly surrounding the tropical ocean basins and in those extratropical regions of the globe that are directly influenced by atmospheric Rossby waves which are excited by variations of tropical deep convection that develop in response to variations in tropical SST (e.g. Hoskins and Schopf 2008).

The most dominant mode of tropical SST variability that is involved in global-scale ocean-atmosphere interactions and teleconnections, especially to Australian climate, is the El Niño-Southern Oscillation (ENSO). The typical SST pattern associated with the warm phase of ENSO (i.e. El Niño) is displayed in Fig.1a, which shows the regression of SST (right panel Fig. 1a) onto the time series of the Nino3 SST index¹ (left panel Fig. 1a). This canonical ENSO accounts for about 65% of the total variance of tropical Pacific SST on seasonal time scales. The second dominant mode of tropical Pacific SST variability, which is known equivalently as Modoki El Niño, central Pacific El Niño, or warm-pool El Niño, explains about 10% of the total SST (Fig. 1b). Here we use the El Niño Modoki SST index (EMI; Ashok et al. 2007)², which is a proxy for the second EOF of tropical SST, to monitor Modoki El Niño. Despite accounting for much less total variance than canonical ENSO, the Modoki El Niño has as large or larger impacts on regional climate especially in Australia (Kumar et al. 2006, Ashok et al. 2007, Wang and Hendon 2007, Kim et al. 2009, Hendon et al. 2009).

In the Indian Ocean, the first dominant mode of the SST variability during late winter to spring season is the Indian Ocean Dipole mode (IOD; Saji et al. 1999). Figure 1c shows the regression of SST onto the Dipole Mode Index (DMI)³, which was defined by Saji et al. (1999) to monitor the IOD. The IOD highly covaries with ENSO especially in spring (as evidenced by the clear indication of El Niño conditions associated with positive IOD in Fig. 1c), and is best understood as a key component of the evolution of ENSO (e.g., Hendon 2003; Dommenges 2010). Although the variations of the IOD that are independent of ENSO are smaller than those associated with ENSO, the sensitivity of Australian climate to SST variations in the Indian Ocean is high, so the smaller independent variations of the IOD are as important to Australian climate as are those that vary dependently with ENSO (e.g. Lim et al. 2009a). This is especially true in winter when the association of the IOD with ENSO is weaker than that in spring (e.g. Cai et al. 2011a).

Successful prediction of seasonal variations of regional climate depends primarily on i) the strength of the teleconnection between the regional climate and dominant modes of tropical SST variability, ii) a forecast system's ability to predict the dominant modes of SST that drive the regional teleconnection, and iii) the forecast model's ability to produce the teleconnections. Australian seasonal climate is primarily impacted by ENSO, El Niño Modoki, and the IOD (e.g. McBride and Nicholls 1983, Wang and Hendon 2007, Meyer et

¹ NINO3 index = $\overline{SST}_{(90^{\circ}\text{W}-150^{\circ}\text{W}, 5^{\circ}\text{S}-5^{\circ}\text{N})}$

² EMI = $\overline{SST}_{(165^{\circ}\text{E}-140^{\circ}\text{W}, 10^{\circ}\text{S}-10^{\circ}\text{N})} - 0.5 * \overline{SST}_{(70^{\circ}\text{W}-110^{\circ}\text{W}, 15^{\circ}\text{S}-5^{\circ}\text{N})} - 0.5 * \overline{SST}_{(125^{\circ}\text{E}-145^{\circ}\text{E}, 10^{\circ}\text{S}-20^{\circ}\text{N})}$

³ DMI = $\overline{SST}_{(50^{\circ}\text{E}-70^{\circ}\text{E}, 10^{\circ}\text{S}-10^{\circ}\text{N})} - \overline{SST}_{(90^{\circ}\text{E}-110^{\circ}\text{E}, 10^{\circ}\text{S}-0^{\circ})}$

al. 2007, Hendon et al. 2009; Cai et al. 2011a). Therefore, skilful prediction of these dominant modes of tropical Indo-Pacific SST variability and a good representation of their teleconnection to Australian climate are prerequisites for skilful prediction of Australian climate.

The aim of this study is to assess the progress of the POAMA seasonal forecast system for improved prediction of Australian climate from the perspective of the prediction and representation of these key climate drivers and their teleconnections. The POAMA system is continuously being developed, with the most recent advances of the POAMA2 system being a new ocean data assimilation system, increased ensemble size, and running multiple versions of the model to better account for model error. A key focus of this study is thus the comparison of forecasts from the new POAMA2 system to the previous version. Although model improvement is the ultimate path toward improved prediction of regional climate, we also explore the benefit of post-processing the forecasts (calibrating) in order to improve reliability of rainfall forecasts over Australia. Furthermore, to shed light onto the progress of the POAMA system development, we also compare POAMA performance to some other contemporary dynamical model forecast systems that have contributed to the EU ENSEMBLES project (Weisheimer et al. 2009). Finally, to explore the benefit of a true multi-model ensemble for Australian rainfall forecasts, we develop and assess a multi-model ensemble forecast by combining forecasts from a subset of the ENSEMBLES models (ECMWF, UK Met Office, and Meteo-France) with the POAMA2 forecast systems.

The key POAMA2 features that have been upgraded over POAMA1.5, including the generation of ocean initial conditions and use of different versions of the model, the retrospective forecast (hindcast) products, and the verification data are described in section 2. Assessment of i) forecast skill for major climate drivers, ii) impact of reducing the model's mean state SST bias, and iii) forecast skill for SEA rainfall based on POAMA2 hindcasts are described in section 3. We also include comparison to the ENSEMBLES models in that section. Lastly, concluding remarks are provided in section 4.

1. POAMA2

The key upgrades of the POAMA2 system over POAMA1.5 are the ocean data assimilation, the use of three slightly different versions of the atmospheric model, and a larger ensemble. In POAMA1.5 the ocean initial conditions were produced from the POAMA Ocean Data Assimilation Scheme (PODAS). PODAS is based on a univariate optimum interpolation (OI) technique of Smith et al. (1991) that assimilates in situ temperature observations in the upper 500 m of the ocean (Wang et al. 2002). Because high quality upper ocean initial conditions are key elements for dynamical ENSO prediction, a major upgrade has been made to POAMA2 by implementing a state-of-the-art ocean data assimilation system called the POAMA Ensemble Ocean Data Assimilation System (PEODAS; Yin et al. 2011). PEODAS assimilates not only ocean temperature but also salinity and generates ensemble of ocean initial conditions. According to Yin et al. (2011), the depiction of the upper ocean in PEODAS is significantly more realistic, accurate and dynamically and thermodynamically consistent than that in PODAS. Furthermore, because the PEODAS assimilation is based on an ensemble technique, an ensemble of perturbed ocean initial conditions is naturally provided for use in ensemble forecast generation.

The POAMA2 forecasts consist of forecasts from three different versions of the coupled model. One version (referred to as P24c) is the same as the model used in POAMA1.5. The other two versions (P24a and P24b) use a slightly different version of the atmospheric model (different treatments of shallow convection) that leads to a reduced mean state bias at longer lead times. However, the mean state bias is not totally eliminated in P24a, so in P24b we have taken the additional step of explicitly controlling the mean state drift by flux correction.

For each version of the P24 model, 10 ensemble members were initialised on the 1st of each month for 1960-2010, and monthly anomalies were computed against the monthly climatology. An ensemble mean forecast was obtained by averaging anomalies of all 30 ensemble members. In contrast, the older P15 system used just 10 ensemble members.

Forecast anomalies were verified against observed anomalies. SST, mean sea level pressure (MSLP) and Australian rainfall forecasts were verified against SST analyses from Hurrell et al. (2008), MSLP analyses from NCEP2 (Kanamitsu et al. 2002) and rainfall analyses from the Australian Water Availability Project (AWAP) monthly gridded rainfall (<http://reg.bom.gov.au/climate/austmaps/metadata-daily-rainfall.shtml>), respectively.

In this study we focus our interest to the forecasts in 1980-2010 when there is less uncertainty in the quality of observational data. This is also the period for which we can compare to the POAMA1.5 forecasts. However, we have generated initial conditions and produced forecasts with POAMA2 for 1960-1979, and some results for this earlier period are provided.

2. RESULTS

2.1 Prediction of climate drivers

In relation to the variability of Australian rainfall, we examined three SST indices - the NINO3 index that depicts SST variations in the equatorial eastern Pacific associated with traditional El Niño events that develop in the Pacific cold-tongue, the EMI that captures SST variations in the equatorial central Pacific associated with warm-pool (Modoki) El Niño development, and the DMI that captures the variation of the Indian Ocean Dipole Mode (e.g., Fig 1). Along with the SST drivers, we also assess the impact of the Southern Annular Mode (SAM), which represents a latitudinal flip-flop in pressure between the mid- and high latitudes of the southern hemisphere (Fig. 1d).

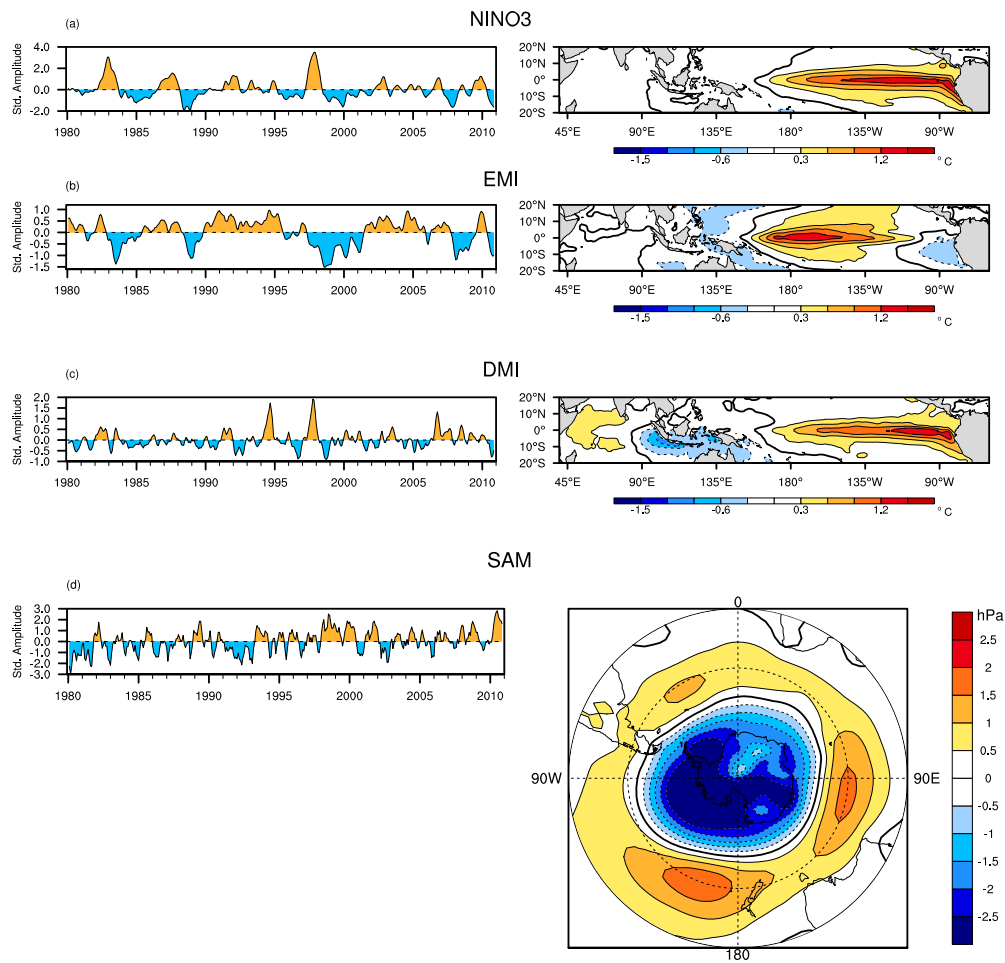


Fig. 1 (a)-(c) Regression patterns (right) of observed SST onto the observed times series of the NINO3, EMI and DMI indices (left) for the period of 1980-2010. (d) Regression pattern of observed MSLP (right) onto the observed SAM index (left) for the same period.

Although the SAM is unlikely to provide much predictability at longer lead times because it is primarily an internally generated atmospheric mode of variability (Limpasuvan and Hartmann 1999), it does have a significant impact on rainfall in south east Australia (Hendon et al. 2007) and therefore can be seen as a primary mechanism that limits predictability at longer lead time. In this study the variability of SAM is represented by the SAM index⁴ proposed by Gong and Wang (1999).

We first assess the dominance of these key drivers of rainfall variability in south east Australia (SEA) by computing the correlation of these indices with the rainfall at each grid point across SEA. We do this in a moving 3 month window and then find the driver that accounts for the most variability (strongest correlation) in each 3 month season. The result is shown as a colour coded map (Fig. 2).

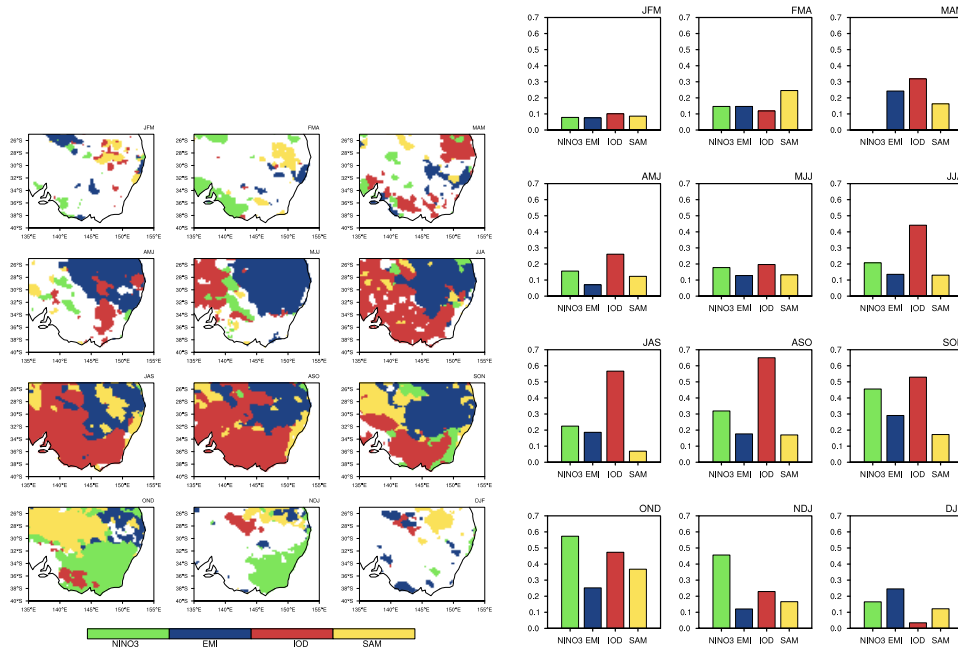


Fig. 2 Climate drivers with highest correlation with rainfall at each grid point (left) and correlation of NINO3 (green), EMI (blue), DMI (red), and SAM index (yellow) with SEA area-averaged rainfall (right) over the period of 1980-2010.

The IOD is seen in Fig. 2 to be the most dominant driver of rainfall variability over the western and southern parts of SEA during winter to spring. According to the study of CAI et al. (2011a), SST over the eastern pole of the IOD excites Rossby waves whose high/low pressure centre is located over the Great Australian Bight and directly affects SEA rainfall. Pressure in the Bight tends to be higher during positive IOD events (cold eastern Indian Ocean), hence rainfall is then lower. The influence of the two different types of El Niño – cold-tongue (Nino3) and warm-pool (EMI) El Niño – is distinctive over SEA: cold-tongue El Niño dominates rainfall variability over the south eastern part of SEA in spring to early summer whereas warm-pool El Niño dominates rainfall variability over

⁴ $SAMI = MSLP_{45^{\circ}S} - MSLP_{60^{\circ}S}$

the north east of SEA in autumn to spring. The SAM is seen to dominate the rainfall variability along the east coast and the north west inland of SEA in winter to late spring.

We now assess the ability of the POAMA2 system to predict these key climate drivers. We do this by forming the Nino3 index, EMI, DMI, and SAM index with the appropriate forecast data from POAMA2 and then verify these predicted indices against the observed indices. POAMA2 demonstrates improved skill to predict both cold-tongue and warm-pool ENSO events compared to POAMA1.5 for the same period of hindcasts (1980-2006) at all lead times (Figs 3a, 3b). The improvement in predicting cold-tongue ENSO is found regardless of forecast start month whereas the improvement in predicting warm-pool ENSO is somewhat limited in the forecasts initialised in the second half of the year (Figs 4a, 4b). In contrast, the prediction of IOD when considered over all start months is less skilful in POAMA2 than POAMA1.5 (Fig. 3c). Nevertheless, forecasts initialised in September and October, which is the time of year when the IOD matures, have better skill in POAMA2 than POAMA1.5 at longer lead times (Fig. 4c). Furthermore, skill to predict SST in the eastern pole of the IOD (IODE) is significantly higher in POAMA2 than POAMA 1.5 with July to December initial conditions (Fig. 4d). This skill improvement in the SST over the eastern pole of IOD is a meaningful achievement as the SST over the eastern pole is an important source of Rossby wave excitation that directly impacts rainfall across southern Australia (e.g. Cai et al. 2011a).

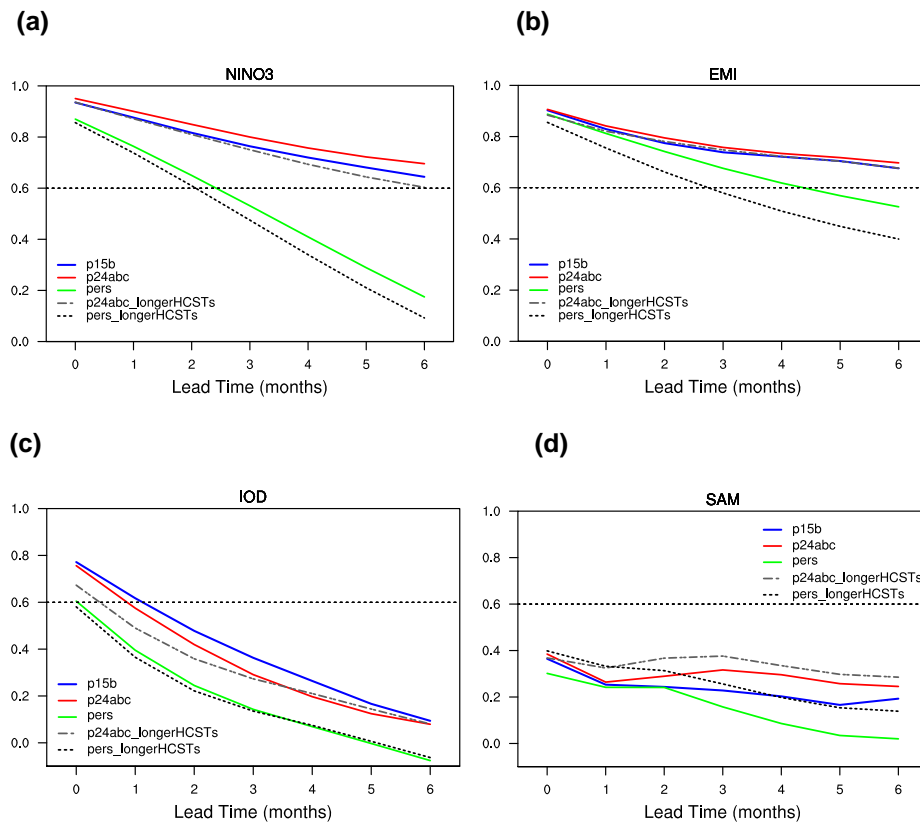


Fig. 3 Forecast skill of key climate drivers Nino3, EMI, IOD, and the SAM. Coloured lines are the forecast skill over 1980-2006, and black lines are the forecast skill over 1960-2010. Forecast skill is assessed by correlation between forecasts and observation of each index.

In addition, we evaluated forecast skill for an extended period from 1960 to 2010 with the POAMA2 system (Fig. 3). Forecasts for NINO3, EMI and DMI over the extended period of 1960-2010 are found to be not as skilful as forecasts in the last 30 years. This poor forecast skill in the earlier 20 years is likely due to the lack of high quality ocean observation and atmospheric data in the pre-satellite era.

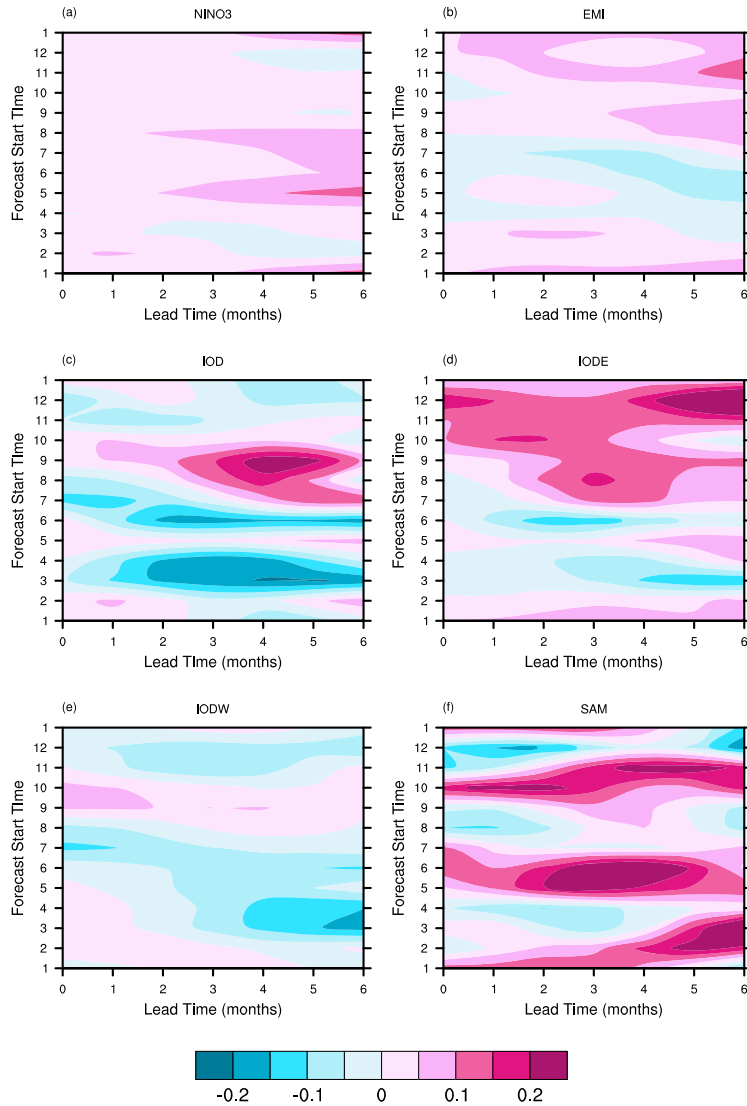


Fig. 4 Forecast skill (correlation between forecasts and observation) difference between POAMA1.5 and POAMA2 (POAMA2 minus POAMA1.5) as a function of forecast start time and lead time. Pink (blue) colour shading indicates POAMA2 skill to be higher (lower) than that of POAMA1.5.

In this project, we have also made a preliminary investigation of the feasibility of predicting the SAM at seasonal timescales (Fig. 3d). As anticipated, forecast skill for the SAM is much lower than for the SST modes. However, there is an indication of improved

skill in POAMA2 over that in POAMA1.5. Interestingly, SAM skill is also higher for the extended forecast period 1960-2010, for which we have no explanation. Although forecast skill of the SAM is limited when all start months are lumped together, longer lead forecasts of SAM appear feasible by POAMA2 for late spring months (Fig. 5a) due to the teleconnection between SAM and ENSO (Fig. 5c; e.g. L'Heureux and Thompson 2006), and spring season SAM is predictable with good skill (i.e. correlation with the observed SAM greater than 0.4) by POAMA2 with up to 2 month lead time (not shown).

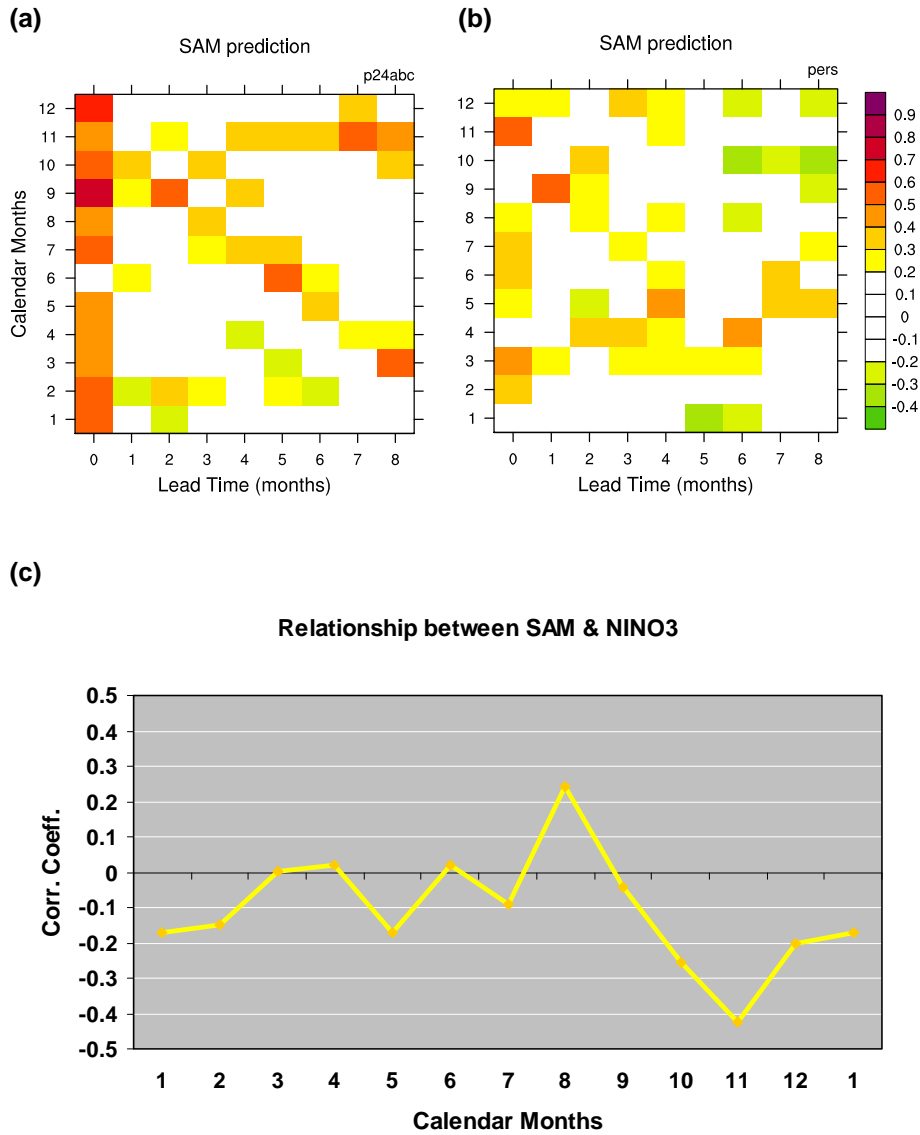


Fig. 5 (a) POAMA2 and (b) persistence forecast skill (as measured by correlation) of SAM as a function of forecast start time and lead time. (c) Observed correlation between monthly SAM and NINO3 in 1980-2010.

Also, it is interesting to note that the monthly SAM can be skilfully predicted by POAMA2 in the first month of the forecasts and is better than a persistence forecast (Figs 5a,b), indicating that the POAMA model is able to represent some aspects of the future evolution of the SAM that depend on the initial conditions (presumably mainly due to atmospheric initial conditions).

The predictability of the key climate drivers of SEA rainfall by POAMA2 are summarized in Fig. 6. NINO3 and EMI, which represent the first two dominant modes of tropical Pacific SST variability and significantly influence SEA rainfall, can be skilfully predicted at least 3 months in advance. In the case of IOD and SAM, there is a large seasonality of forecast skill, but good forecast skill is found in the spring seasons when IOD and SAM are important to SEA rainfall as shown in Figure 2.

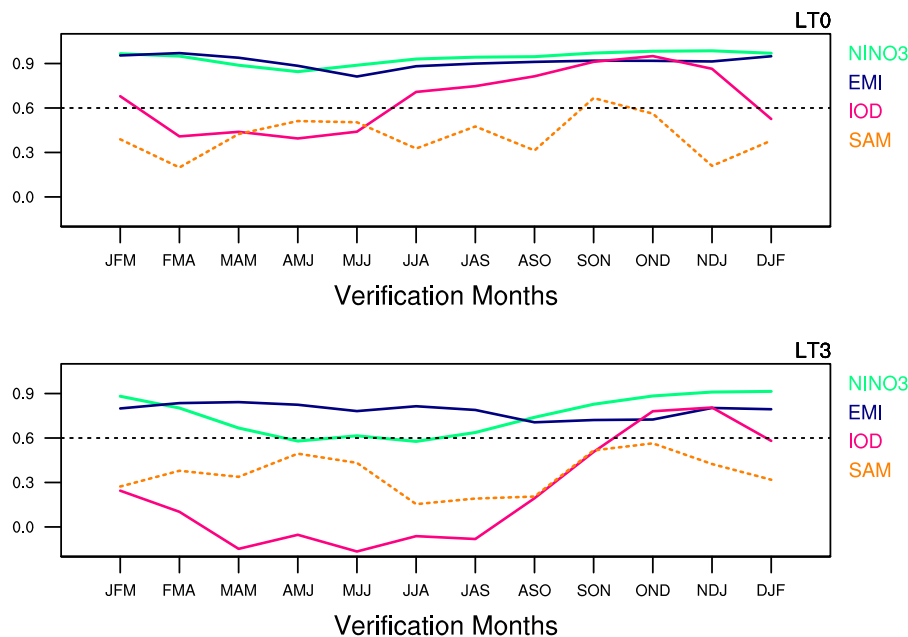


Fig. 6 Forecast skill (as measured by correlation) for major climate drivers at lead time zero month (upper panel) and three months (lower panel). The verification season (3 month mean) is along the x-axis.

2.2 Impact of flux correction

A common problem with coupled seasonal forecast models such as POAMA is that model climate drifts as forecast lead time increases. In the case of POAMA, a tropical-wide cold SST bias develops together with a warm SST bias off the west coast of South America, and these biases grow rapidly during the first 6 months of the forecast with biases in the mean state SST ranging from -4° to 6°C (Figs 7a,d). In terms of seasonal climate prediction, these mean state SST biases negatively impact skilful prediction of ENSO by shifting the location of maximum SST variability associated with ENSO to the west of the observed location, and therefore, hindering the model's ability to discern different types of ENSO events at long lead times (Hendon et al. 2009). Furthermore, the atmosphere and oceanic teleconnections of ENSO to the Australian region are negatively impacted by these biases. For instance, Lim et al. (2009b) reported that the relationship between ENSO and

Australian winter rainfall is oppositely simulated to the observed relationship at lead times longer than a couple of months.

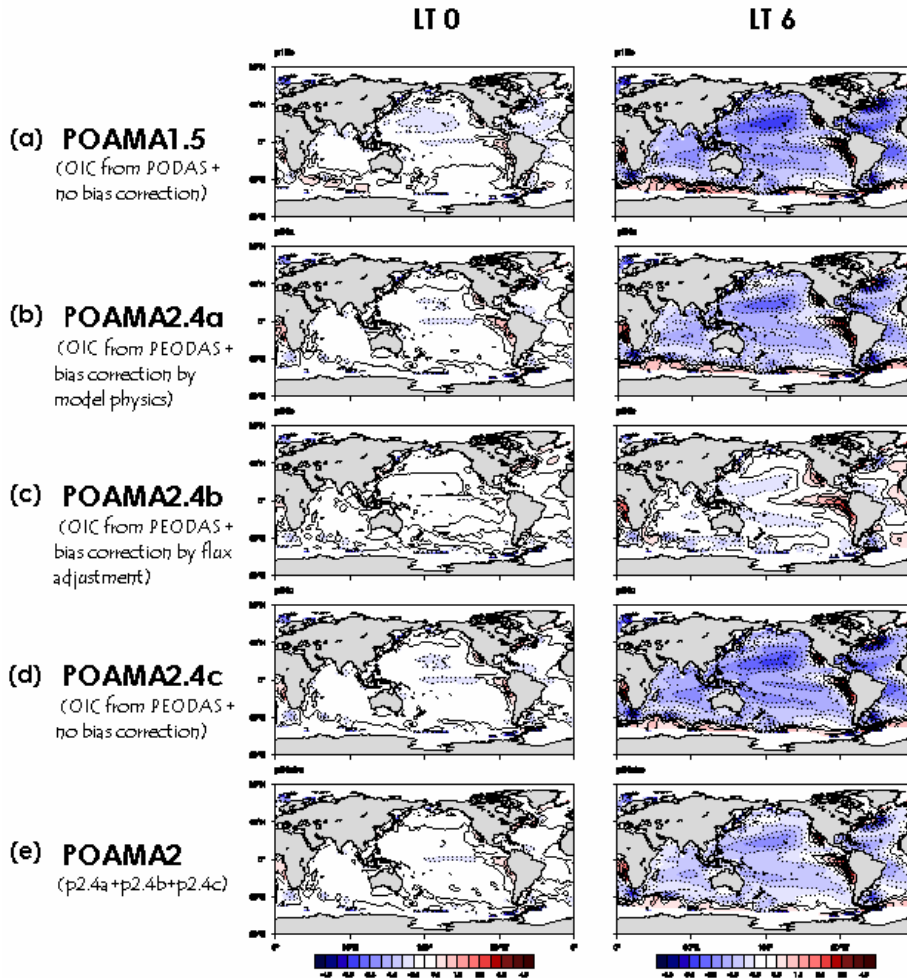


Fig. 7 SST mean state bias at 0 and 6 month lead times in POAMA1.5, each version of POAMA2 and the finally configured POAMA2 consisting of the three versions of POAMA2. Blue colour indicates predicted climatological SST to be colder than the observed over the period of 1980-2006. Contour interval is 0.5 °C.

In POAMA2, cold and warm SST biases are reduced by two distinct approaches. In P24a we used a slightly different treatment of shallow convection that resulted in slightly less model drift compared to P24c (Fig. 7b). In P24b, which has the same convection scheme as P24a, we used an explicit flux correction scheme (Lim et al. 2010) that virtually eliminated all of the drift in the surface climate (Fig. 7c). The flux correction effectively reduces the cold bias to less than -1°C over the wide tropical Pacific, thereby improving the model's ability to simulate the spatial patterns of different types of ENSO as follows. Figure 8 shows the ability of P24a (non-flux corrected) and P24b (flux corrected) to simulate the observed patterns of SST variability associated with warm-pool and cold-tongue El Niño events. The correlation of the observed patterns is only 0.4, which suggests that the two types of El Niño are distinctive in terms of pattern. The correlation between the predicted

patterns is much higher than the observed in both non-flux corrected and flux corrected forecasts, which indicates the model's ability to simulate these two different flavoured El Niño events falls short. Nevertheless, the flux corrected forecasts better distinguish the spatial patterns of the two types of El Niño, simulating the pattern of each type of El Niño to be closer to its observed counterpart (Figs. 8c,d). For the flux corrected model, the pattern correlation between the predicted and observed EMI is higher than the pattern correlation between the predicted NINO3 and EMI at least at up to two month lead time (Fig. 8d), which implies that warm-pool El Niño patterns are predictable with clear distinction from cold-tongue El Niño about two months in advance. This amounts to about a month improvement in lead time over the non-flux corrected model.

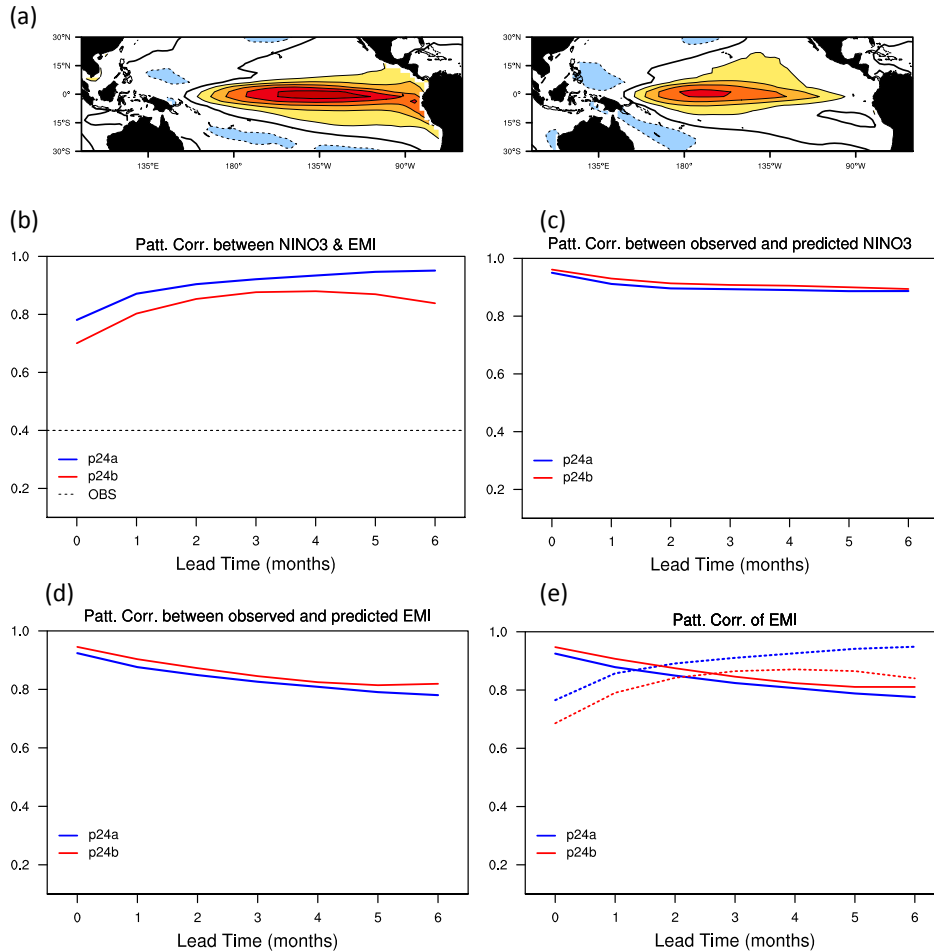


Fig. 8 (a) SST patterns of cold-tongue El Niño (left) and warm-pool El Niño (right), (b) pattern correlation between cold-tongue and warm-pool El Niños in the observation (dashed line), and non flux corrected (p24a; blue line) and flux corrected (p24b; red line) forecasts, (c) pattern correlation between predicted and observed cold-tongue El Niño, and (d) the same as (c) but for warm-pool El Niño, (e) overlapped plot of (b) and (d). In (e) the cross point of the solid and dashed lines indicates the lead time when the model predicted cold-tongue and warm-pool El Niños start to be more alike to each other than to their observed counterparts.

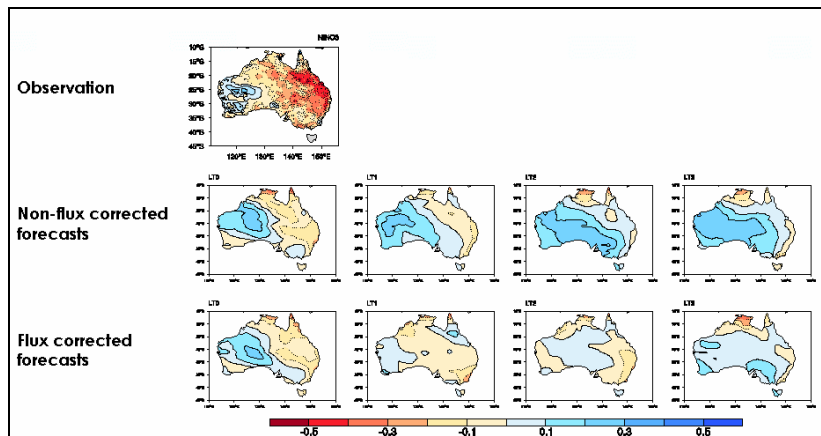
Meaningful improvements in the teleconnection between ENSO and Australian winter rainfall are also found in the flux corrected forecasts. We assess this by computing the correlation of Australian rainfall with the Niño3 and EMI indices from the forecasts and observations (Figs. 9a,b). Although the observed historical relationship shows that the eastern part of Australia experiences rainfall deficit with the development of cold-tongue El Niño during austral winter, the non-flux corrected POAMA2 spuriously simulates rainfall surplus during cold-tongue El Niño over most of the continent (Fig. 9a). This bias in the ENSO teleconnection tends to get worse with increasing forecast lead time. Also, the strong relationship between eastern Australian winter rainfall and warm-pool El Niño in the observation is underestimated in the non-flux corrected forecasts after a month from the initialisation (Fig. 9b).

Flux correction alleviates these biases by keeping the dry conditions in the east during cold-tongue and warm-pool El Niño events at up to 2 month lead times. These improvements in the El Niño teleconnection contribute to higher forecast skill for eastern Australian rainfall in winter by about 2 month lead time (Fig. 9c).

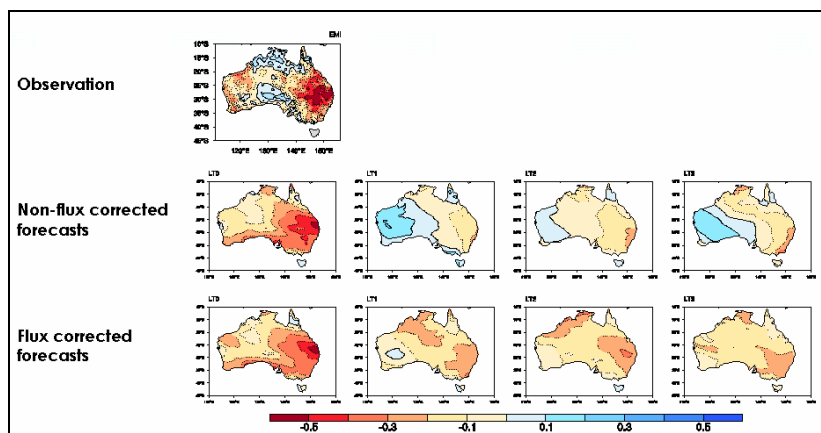
Flux correction also improves the model's representation of the mean position and intensity of subtropical ridge (STR) over Australia. The position and intensity of the STR is strongly tied to rainfall variability in eastern Australia (e.g., Drosowsky 2005). The influence of the STR on rainfall over the southern part SEA (south of 32°S) is demonstrated by the correlation of rainfall with the intensity and position of the STR as provided by the Drosowsky (2005) L-index (Fig. 10a). The correlation with rainfall peaks in winter but is strong in late autumn to early spring (see also Cai et al. 2011b). Both non-flux corrected and flux corrected forecasts have a bias of STR position that is displaced about 1-2 degree equatorward of the observed position in summer to autumn seasons early in the forecasts (Fig. 10b). However, the bias in the mean position of the ridge grows significantly in the non-flux corrected version as lead time increases. For instance, the predicted STR is positioned poleward of the observed during late winter to spring while it is positioned equatorward of the observed during summer to early autumn. Furthermore, the predicted STR intensity is overestimated during late autumn to spring but underestimated during summer in the non-flux corrected version. Although flux correction is unable to eliminate all of these biases, it significantly reduces the magnitudes of them at long lead times (4-6 months). Additionally, prediction of the interannual variations of the STR intensity and position by POAMA2 (assessed by correlation of predicted against observed and shown in Fig. 10b as dot/crosses whose size is proportional to the correlation) seems possible only to lead times less than 2 months.

Despite some key benefits of flux correction, the forecasts of ENSO and the IOD from the flux corrected model are slightly less skilful than those from the non-flux corrected model (Lim et al. 2010). This competing biases/forecast skill from the different versions of the model is the key reason we combined the three different versions of POAMA2.

(a)



(b)



(c)

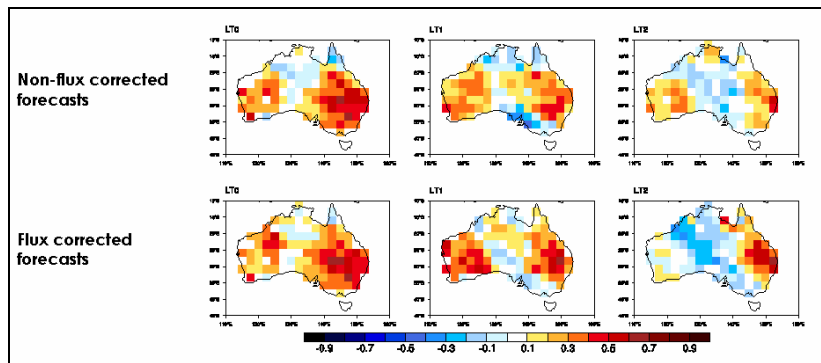


Fig. 9 Correlation of June-July-August Australian rainfall with (a) the NINO3 index and (b) the EMI in the observation and in the non-flux corrected and flux corrected forecasts at lead time of 0-4 months over the period of 1980-2010. (c) Forecast skill (as measured by correlation) of winter rainfall at 0-2 month lead time.

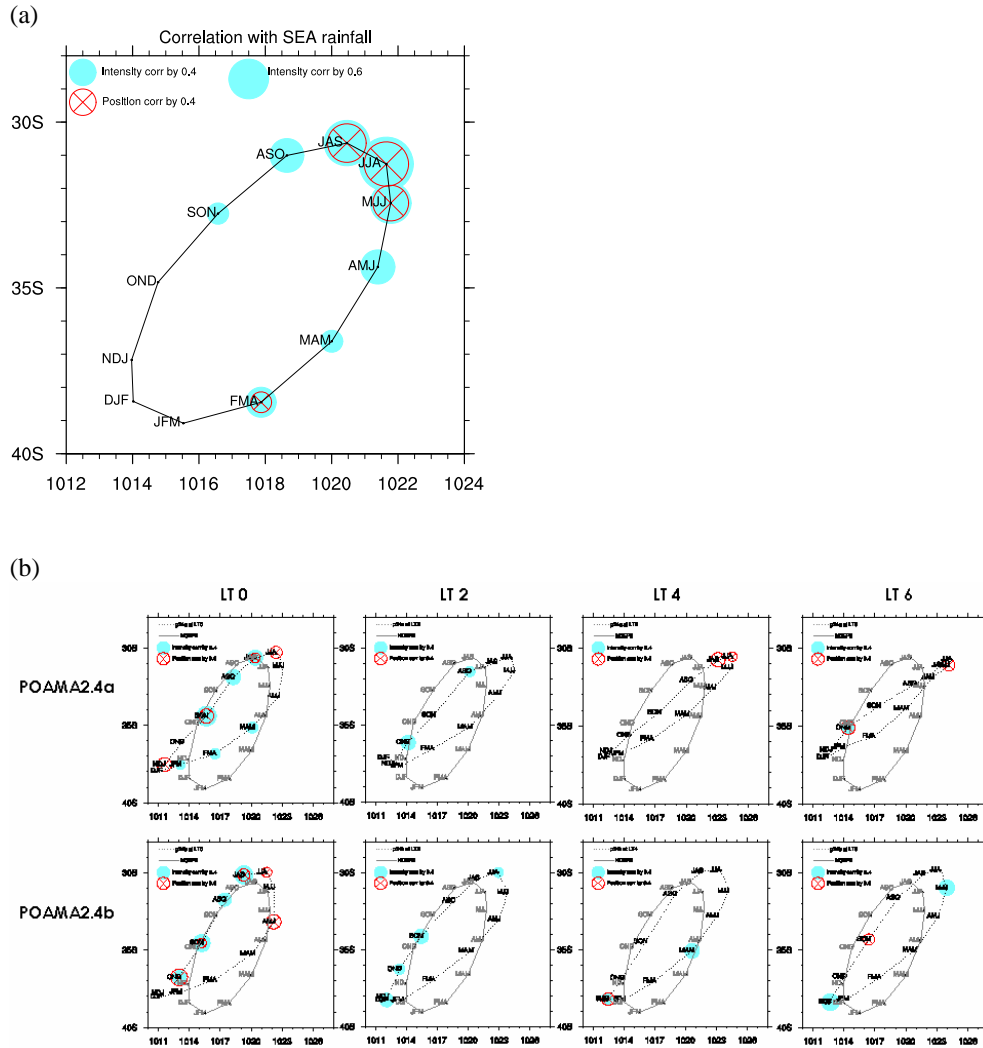


Fig. 10 (a) Observed seasonal cycle of subtropical ridge (STR) mean position (y-axis) and intensity (x-axis) and their correlation with the southern part of SEA rainfall (south of 32°S) superimposed on the cycle at each season. Blue circle (red open circle with x) represents the correlation with STR intensity (position). In the legend the small and big blue circles represents 0.4 and 0.6 correlation, respectively, (b) Representation of STR mean intensity and position and prediction skill of the variabilities of STR intensity and position in non-flux corrected (upper row) and flux corrected (bottom row) forecasts at lead times of 0, 2, 4, and 6 months. Solid grey line represents observed seasonal cycle whereas dotted black line represents predicted seasonal cycle. Blue circle (red open circle) indicates skill to predict STR intensity (position) variability. Dot size is proportional to the magnitude of correlation coefficient. The size of the circles in the legend represent 0.4 correlation.

2.3 SEA rainfall forecasts

Rainfall forecast skill is assessed in terms of probabilistic forecasts for rainfall being above the median, and the skill is scored with proportion correct (i.e. proportion of correct forecasts to the total forecasts; also commonly called hit rates). We deem the forecast system to be skilful if it correctly predicts the occurrence of above median rainfall more than 55% of the time. Probabilistic forecasts from the models were computed with 9 ensemble members of POAMA1.5 and of each of the three versions of POAMA2. Final POAMA2 probabilistic forecasts were from averaging the three sets of probabilistic forecasts from the three versions of POAMA2. We compute the proportion correct in sliding 3 month seasons for 0 month lead time (Fig. 11a) and 3 month lead time (Fig. 11b). At 0 month lead time SEA seasonal rainfall is skilfully predicted (i.e. proportion correct greater than 55%) by both POAMA1.5 (left column in Fig. 11a) and POAMA2 (middle column in Fig. 11a) for all seasons except for late autumn (May-July) and summer (December-February). The forecasts are skilful out to 3 month lead times for late winter to early summer (Fig. 11b). The proportion correct of rainfall forecasts is comparable between POAMA1.5 and POAMA2. However, another key aspect of the forecasts is its reliability. Reliability refers to the capability of the model to predict forecast frequencies with the correct climatological distribution and is assessed with an attributes diagram (Fig. 12). POAMA2 is seen to have slightly higher forecast reliability than POAMA1.5, which we attribute to the combination of three different versions of the model and the increased ensemble size used in POAMA2. Nevertheless, the reliability of POAMA2 forecasts is far from being perfect: POAMA2 probabilistic forecasts still demonstrate over-confident characteristics (e.g., the forecasts predict occurrences/non-occurrences of above median rainfall more often than is observed).

Deleted:

This lack of improved reliability of POAMA2 compared to POAMA1.5 has motivated us to explore the benefits of post-processing the forecasts. We do so using the calibration technique of inflation of variance (e.g., Johnson and Bowler 2009). This technique adjusts the forecast spread of the ensemble in an optimum fashion so that the statistical characteristics of each ensemble member are indistinguishable from reality. This technique ensures that the variance of the individual forecast members is equal to the observed variance but does the adjustment in a fashion that minimizes the root mean square error of the ensemble mean forecast. However, the calibration technique depends on historical relationships with observed data, so the application require cross-validation in order to provide a true estimate of the value of the technique when applied to future forecast data. The generally low correlation between forecasts and observation means that many of the benefits of calibration do not survive cross validation. Nonetheless, Charles et al. (2011) have shown some good benefit of calibration when applied to POAMA1.5.

The calibrated POAMA2 forecasts show similar forecast accuracy as the uncalibrated forecasts (Fig. 11 third column) – e.g. no systematic change in the proportion correct as a result of calibration – but do show improved reliability out to longer lead times of more than 3 months (Fig.12 third column). However, forecast sharpness (the range of forecast probability) and resolution (the degree to which different probability forecasts followed by different observed outcomes) are, not surprisingly, reduced.

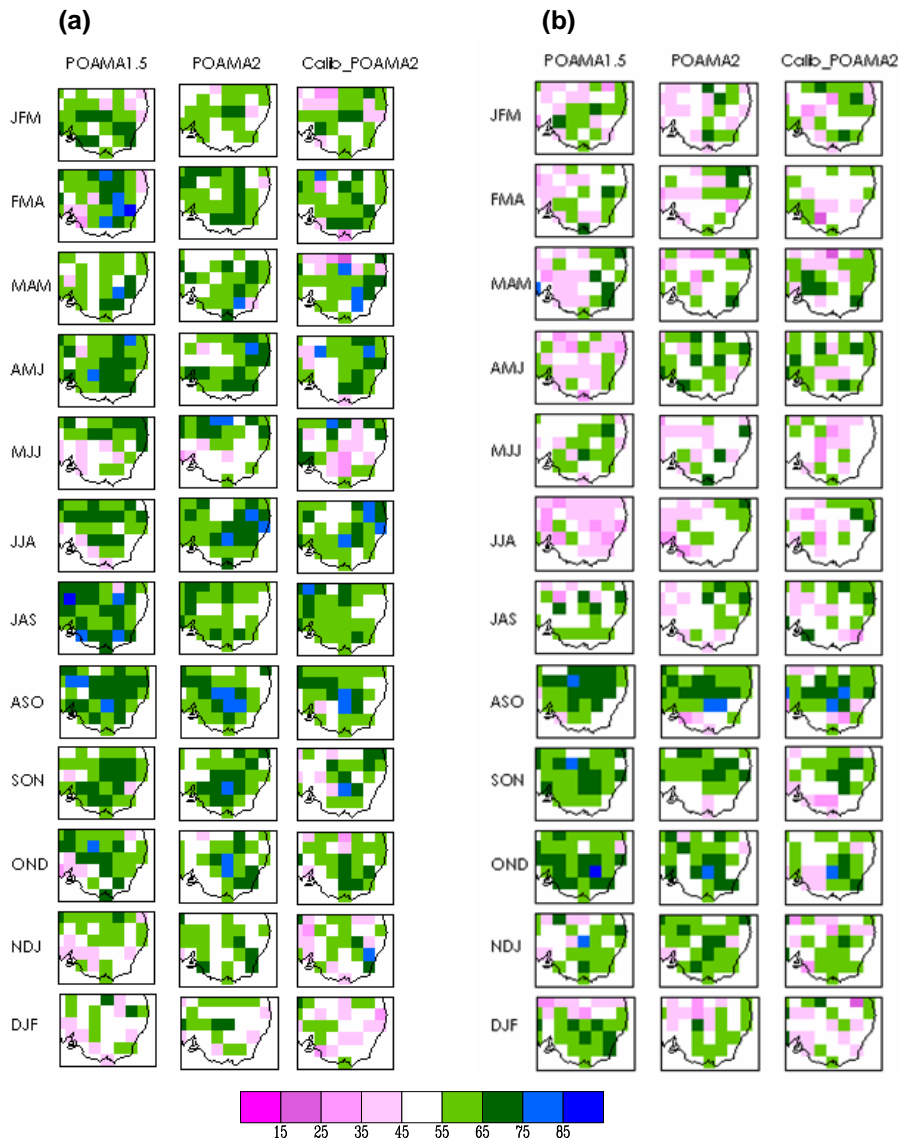


Fig. 11 Proportion of correct forecasts (expressed in percentage) of predicting seasonal rainfall to be above the median in POAMA1.5 (left column), POAMA2 (middle column) and calibrated POAMA2 (right column) at (a) LT 0 and (b) LT 3 months. Colour shading is 10% interval.

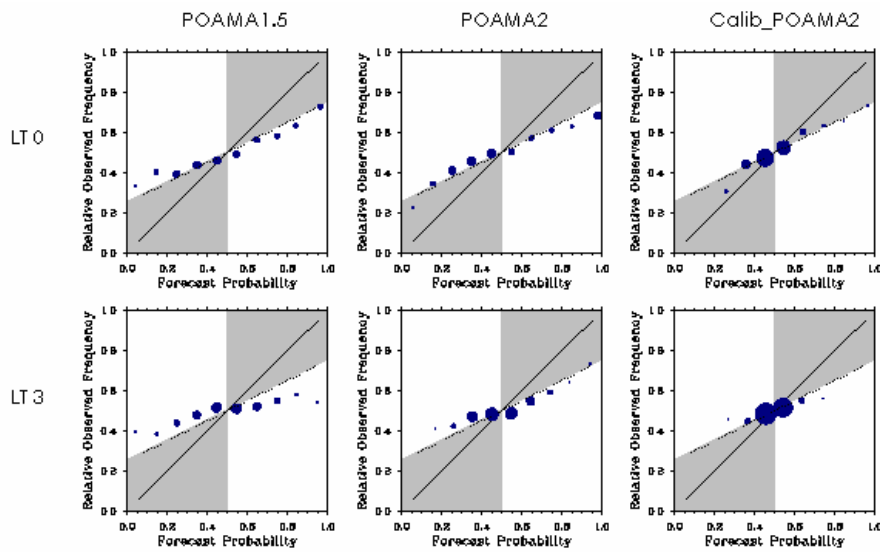


Fig. 12 Attributes diagrams of POAMA1.5, POAMA2 and calibrated POAMA2 forecasts of above median rainfall, considering the forecasts over all grid points of SEA for all 12 seasons in 1980-2006 at LT 0 (upper panels) and LT 3 months (lower panels). Perfectly reliable forecasts should line up with the diagonal line. Forecasts in the grey areas are considered to be reliable as they are correct in predicting the occurrence/non-occurrence of an event (in this study, above median rainfall) and their errors are smaller than a climatological forecast. The size of dots represents forecast frequency in each probabilistic forecast category.

2.4 Comparison with ENSEMBLES and a true MME

Finally, we compare the POAMA2 forecasts to some of the models that contributed to the ENSEMBLES project (Weisheimer et al. 2009) in order to see where POAMA2 sits in comparison with other state-of-the-art seasonal forecast models. This comparison will highlight common problems, flag where POAMA is lagging behind and can also be used to assess the benefit of a real multi-model ensemble for Australian rainfall forecasts. Six sets of 9 member ensemble hindcasts from different European seasonal forecast systems were available on the ENSEMBLE website (<http://www.ensembles-eu.org/>). The hindcasts were initialised on the first day of February, May, August and November and ran for 6 months. For the current study, we chose forecasts from the ECMWF system3, UK Met Office HadGEM2-A, and Meteo-France ARPEGE4.6 to compare with POAMA2 for their forecast skill for SEA rainfall. These three systems contribute to the real-time EUROSIP project and so are indicative of the capability of current real-time system used in the EU. We analysed 1 month lead forecasts to predict the four main seasons – Mar-May, June-August, September-November, and December-February.

(a)

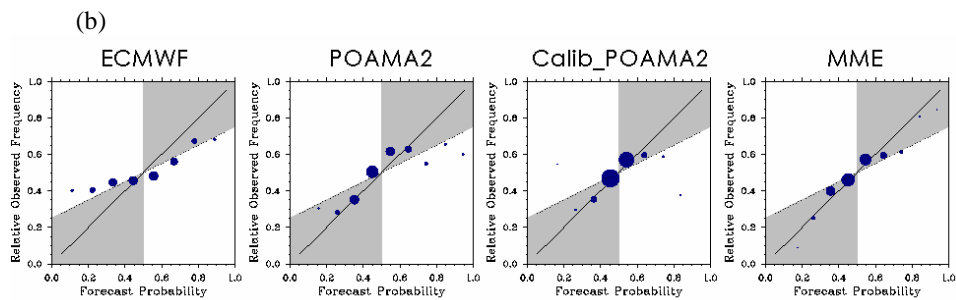
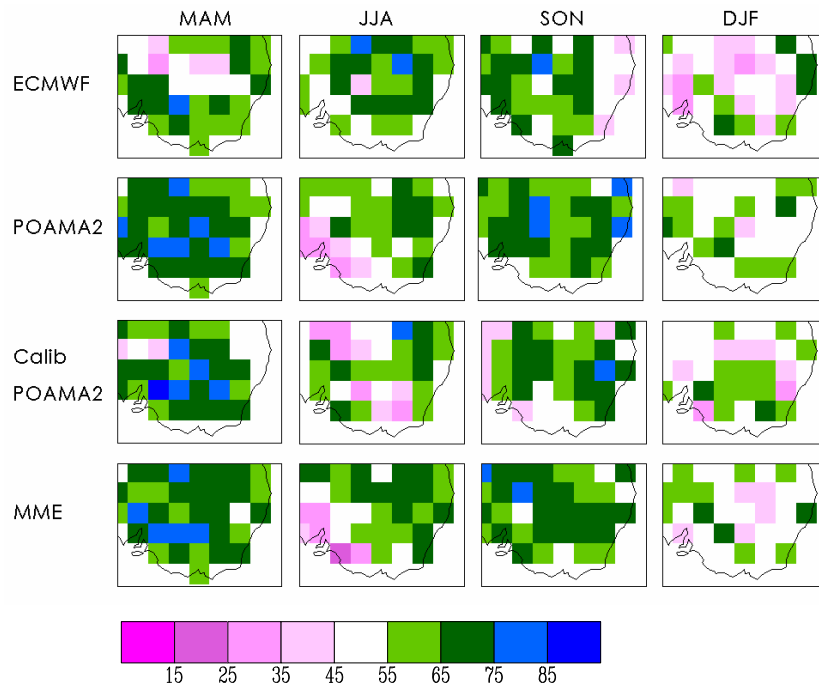


Fig. 13 (a) Proportion of correct forecasts and (b) attributes diagrams of predicting seasonal rainfall over SEA to be above the median in ECMWF system3, POAMA2, calibrated POAMA2 and a multi-model ensemble system consisting of POAMA2, ECMWF, UK Met Office, and Meteo-France forecast systems at 1 month lead time.

Our investigation of the ENSEMBLES models suggests that the ECMWF system3 has higher skill in predicting SEA rainfall than any single version of POAMA2 (Langford and Hendon 2011). But the single versions of POAMA2 are as good or better than any of the other models. However, the full 27 member ensemble of POAMA2 has comparable skill or even slightly higher skill than ECMWF system3 over the SEA region in terms of proportion correct (Fig. 13a). Also, the POAMA2 forecasts for above median rainfall for the major four seasons are highly reliable in the range of probabilities between 20-70% probabilities, and POAMA2 forecast reliability is stretched further by calibration (Fig.13b).

The benefit of a true multi-model ensemble was explored by combining the forecasts from POAMA2, ECMWF, UK Met Office and Meteo-France. As shown by the proportion

correct for above median rainfall (Fig. 13a), the MME is the best system compared to both POAMA2 and ECMWF system³. Furthermore, the MME approach greatly improves forecast reliability (Fig. 13b). But a key additional benefit of the MME is that reliability is improved without loss of resolution and sharpness, and so the MME is a significant improvement over calibration of a single model. This benefit of the MME occurs because independent information from each model is added to the forecast system (Stephenson et al. 2005; Doblas-Reyes et al. 2006). Therefore, a key conclusion of this assessment is that given the current capability of dynamical models, a MME approach seems the best way of improving seasonal forecast skill and quality for Australian rainfall over SEA.

3. CONCLUDING REMARKS

Our investigation shows that the POAMA2 system has improved skill in predicting variability of different types of ENSO and SST in the eastern pole of IOD, which is strongly associated with SEA rainfall variability in winter and spring. We attribute this increase in skill over the POAMA1.5 system to the improved ocean initial conditions provided by the PEODAS ocean assimilation system.

We showed some benefit of reducing the model's mean state SST bias in one version of POAMA2 (P24b). The reduced mean state bias improved the simulation of spatial patterns of cold-tongue and warm-pool El Niños and the representation of their teleconnection on Australian winter rainfall. Although forecasts from the flux corrected model P24b demonstrate improved performance for representing key atmospheric teleconnection, the predictions of ENSO and the IOD from P24b are not as skilful as those from the non-flux corrected versions. Therefore, the final version of POAMA2 consists of both a flux corrected and non flux corrected versions in order to incorporate the benefits of flux correction to the forecasts without lowering the prediction skill of ENSO and IOD too much.

Forecast skill of SEA seasonal rainfall from POAMA2 is comparable to the skill of POAMA1.5 for the proportion correct of rainfall exceeding the median, but POAMA2 forecasts show slightly better reliability than POAMA1.5 due to the increased ensemble size. Forecast reliability can be further improved by calibrating the forecasts with an inflation of variance technique. This technique significantly improves forecast reliability without reducing forecast accuracy but at the expense of loss of forecast resolution and sharpness.

Assessment of some contemporary seasonal forecast systems in Europe demonstrates that the POAMA2 system is on par with the other state-of-the-art systems. In particular, POAMA2 has similar forecast accuracy and all models suffer from similar lack of reliability. As such, a multi-model ensemble consisting of POAMA2, ECMWF, UK Met Office and Meteo-France forecast systems demonstrates that a MME is the best possible method of providing improved forecasts of SEA climate. The MME improves accuracy and reliability while retaining sharpness and resolution.

4. ACKNOWLEDGMENTS

This research was supported in part by the South Eastern Australian Climate Initiative (SEACI; <http://www.seaci.org>; Advancing Seasonal Predictions for SEA) and by the WIRADA initiative. The authors are grateful to Dr William Wang in the Climate and Weather and Dr Aihong Zhong in the NMOC for their useful comments on this manuscript.

5. REFERENCES

- Anderson, D.L.T. 2008. *Overview of seasonal forecasting. Seasonal Climate: Forecasting and managing risk*. A. Troccoli, M. Harrison, D. L. T. Anderson and S. J. Mason, Eds., Springer Academic Publishers, 47-68.
- Ashok, K., Behera, S.K., Rao, S.A. and Weng, H. 2007. El Niño Modoki and its possible teleconnection. *J. Geophys. Res.*, **112**, C1107, doi:10.1029/2006JC003798.
- Cai, W., Rensch, P.V., Cowan, T. and Hendon, H.H. 2011a. Teleconnection pathways for ENSO and the IOD and the mechanism for impacts on Australian rainfall. *J. Climate*, doi:10.1175/2011JCLI4129.1
- Cai, W., Rensch, P.V. and T. Cowan, 2011b. Influence of global-scale variability on the subtropical ridge over southeast Australia. Accepted to *J. Climate*.
- Charles, A., Hendon, H., Wang, Q. J., Robertson, D. and Lim, E.-P. 2011. Comparison of Techniques for the calibration of coupled model forecasts of Murray-Darling Basin seasonal mean rainfall. *CAWCR Technical Report No. 40*.
- Colman, R., Deschamps, L., Naughton, M., Rikus, L., Sulaiman, A., Puri, K., Roff, G., Sun, Z. and Embury, G. 2005. BMRC Atmospheric Model (BAM) version 3.0: Comparison with mean climatology. *BMRC Research Report No. 108*, Bureau of Meteorology Research Centre, 32 pp.
(available from <http://www.bom.gov.au/bmrc/pubs/researchreports/researchreports.htm>).
- Doblas-Reyes, F.J., Hagedorn, R., Palmer T.N. and Morcrette, J.-J. 2006. Impact of increasing greenhouse gas concentrations in seasonal ensemble forecasts. *Geophys. Res. Lett.*, **33**, L07708, doi:10.1029/2005GL025061.
- Dommenget, D. 2010. An objective analysis of the observed spatial structure of the tropical Indian Ocean SST variability. *Clim. Dyn.*, **36**, 2129–2145.
- Drosowsky, W. 2005: The latitude of the subtropical ridge over Eastern Australia: the L-index revisited. *Int. J. Climatol.*, **25**, 1291-1299.
- Gong, D. and Wang, S. 1999. Definition of Antarctic Oscillation index, *Geophys. Res. Lett.*, **26**(4), 459–462, doi:10.1029/1999GL900003.
- Hendon, H.H. 2003. Indonesian rainfall variability: Impacts of ENSO and local air-sea interaction. *J. Climate*, **16**, 1775-1790.
- Hendon, H.H., Thompson, D.W.J. and Wheeler, M.C. 2007. Australian rainfall and temperature variations associated with the Southern Hemisphere Annular Mode. *J. Climate*, **20**, 2452-2467.
- Hendon, H.H., Lim, E.-P., Wang, G., Alves O. and Hudson D. 2009. Prospects for predicting two flavours of El Niño. *Geophys. Res. Lett.*, **36**, L19713, doi:10.1029/2009GL040100.

- Hoskins, B. and Schopf, P. 2008. *Ocean-Atmosphere basis for seasonal climate forecasting. Seasonal Climate: Forecasting and managing risk*. A. Troccoli, M. Harrison, D. L. T. Anderson and S. J. Mason, Eds., Springer Academic Publishers, 69-92.
- Hudson, D., Alves, O., Hendon, H.H. and Wang, G. 2010. The impact of atmospheric initialisation on seasonal prediction of tropical Pacific SST. *Climate Dyn.*, doi:10.1007/s00382-010-0763-9.
- Hurrell, J.W., Hack, J.J., Shea, D., Caron, J.M. and Rosinski, J. 2008. A new sea surface temperature and sea ice boundary data set for the Community Atmosphere Model. *J. Climate*, **21**, 5145-5153, doi: 10.1175/2008JCLI2292.1.1
- Johnson, C. and Bowler, N. 2009. On the reliability and calibration of ensemble forecasts. *Mon. Wea. Rev.*, **137**, 1717-1720.
- Kanamitsu, M., Kistler, R.E., Reynolds, R.W., Yang, S.-K., Hnilo, J.J., Fiorino, M. and Potter, G.L. 2002. NCEP/DOE AMIP-II Reanalysis (R-2). *Bull. Amer. Meteor. Soc.*, **83**, 1641–1643.
- Kim, H.-M., Webster, P.J. and Curry, J.A. 2009. Impact of shifting patterns of Pacific Ocean warming on North Atlantic tropical cyclones, *Science*, **325**, 77– 80, doi:10.1126/science.1174062.
- Kumar, K.K., Rajagopalan, B., Hoerling, M., Bates, G., and Cane, M. (2006). Unraveling the mystery of Indian monsoon failure during El Niño, *Science*, **314**, 115– 119, doi:10.1126/science.1131152.
- Langford, S. and Hendon, H.H. 2011. Assessment of international seasonal rainfall forecasts for Australia and the benefit of multi-model ensembles for improving reliability. *CAWCR Technical Report No. 39*.
- L'Heureux, M.L. and Thompson, D.W.J. 2006. Observed Relationships between the El Niño–Southern Oscillation and the Extratropical Zonal-Mean Circulation. *J. Climate*, **19**, 276–287.
- Lim, E.-P., Hendon, H.H., Hudson, D., Wang G. and Alves, O. 2009a. Dynamical forecast of inter-El Niño variations of tropical SST and Australian spring rainfall. *Mon. Wea. Rev.* **137**, 3796-3810.
- Lim, E.-P., Hendon, H.H., Alves, O., Yin, Y., Zhao, M., Wang, G., Hudson, D. and Liu, G. 2009b. Impact of SST bias correction on prediction of ENSO and Australian winter rainfall. *CAWCR Res. Lett.*, **3**, iv.
- Lim, E.-P., Hendon, H.H., Alves, O., Yin, Y., Wang, G., Hudson, D., Zhao, M. and Shi, L. 2010. Dynamical seasonal prediction of tropical Indo-Pacific SST and Australian rainfall with improved ocean initial conditions. *CAWCR Technical Report No. 32*
- Lim, E.-P., Hendon, H.H., Anderson, D.L.T., Charles A. and Alves O. 2011. Dynamical, statistical-dynamical, and multimodel ensemble forecasts of Australian spring season rainfall. *Mon. Wea. Rev.*, **139**, 958-975.
- Limpasuvan, V. and Hartmann. D.L. 1999. Eddies and the annular modes of climate variability. *Geophys. Res. Lett.*, **26**, 3133-3136.

- McBride, J.L., and Nicholls, N. 1983. Seasonal relationships between Australian rainfall and the Southern Oscillation. *Mon. Wea. Rev.*, **111**, 1998–2004.
- Meyers, G., MacIntosh, P., Pigot, L. and Pook, M. 2007: The Years of El Niño, La Niña, and Interactions with the Tropical Indian Ocean. *J. Climate*, **20**, 2872-2880.
- Oke, P.R., Schiller, A., Griffin, D.A. and Brassington, G.B. 2005. Ensemble data assimilation for an eddy-resolving ocean model of the Australian region. *Q. J. Roy. Met. Soc.*, **131**, 3301-3311.
- Saji, N., Goswami, B.N., Vinayachandran, P.N. and Yamagata, T. 1999. A dipole mode in the tropical Indian Ocean. *Nature*, **401**, 360–363.
- Schiller, A., Godfrey, J.S., McIntosh, P.C., Meyers, G., Smith, N.R., Alves, O., Wang, G. and Fiedler, R. 2002. *A New Version of the Australian Community Ocean Model for Seasonal Climate Prediction*. CSIRO Marine Research Report No. 240.
- Smith, N.R., Blomley, J.E. and Meyers, G. 1991. A univariate statistical interpolation scheme for subsurface thermal analyses in the tropical oceans. *Prog. Oceanog.*, **28**, 219-256.
- Stephenson, D.B., Coelho, C.A.D.S., Doblas-Reyes, F.J. and Balmaceda, M. 2005. Forecast assimilation: A unified framework for the combination of multimodel weather and climate predictions. *Tellus*, **57A**, 253-264.
- Uppala, S.M. and Coauthors, 2005. The ERA-40 re-analysis. *Quart J. Roy Met Soc*, **131**, 2961-3012.
- Valke, S., Terray, L. and Piacentini, A. 2000. The OASIS coupled user guide version 2.4, Technical Report TR/ CMGC/00-10, CERFACS.
- Wang G., Kleeman, R., Smith, N. and Tseitkin, F. 2002. The BMRC coupled general circulation model ENSO forecast system. *Mon. Wea. Rev.* **130**, 975-991.
- Wang, G. and Hendon, H.H. 2007. Sensitivity of Australian rainfall to inter-El Niño variations. *J. Climate*, **20**, 4211–4226.
- Weisheimer, A., Doblas-Reyes, F.J., Palmer, T.N., Alessandri, A., Arribas, A., Deque, M., Keenlyside, N., MacVean, M., Navarra, A. and Rogel, P. 2009. ENSEMBLES: A new multi-model ensemble for seasonal-to-annual predictions—Skill and progress beyond DEMETER in forecasting tropical Pacific SSTs. *Geophys. Res. Lett.*, **36**, L21711, doi:10.1029/2009GL040896.
- Yin, Y., Alves, O. and Oke, P. 2011: An ensemble ocean data assimilation system for seasonal prediction. *Mon. Wea. Rev.*, **139**, 786-808.



The Centre for Australian Weather and
Climate Research is a partnership between
CSIRO and the Bureau of Meteorology.